Journal of Colloid and Interface Science 641 (2023) 585–594

Contents lists available at ScienceDirect

Journal of Colloid and Interface Science

journal homepage: www.elsevier.com/locate/jcis

Drop splashing after impact onto immiscible pools of different viscosities

Ben D. Fudge [a], Radu Cimpeanu [b,c,d], Arnaud Antkowiak [e], J. Rafael Castrejón-Pita [f], Alfonso A. Castrejón-Pita [a,*]

[a] Department of Engineering Science, University of Oxford, Oxford OX1 3PJ, United Kingdom
[b] Mathematics Institute, University of Warwick, Coventry CV4 7AL, United Kingdom
[c] Mathematical Institute, University of Oxford, Oxford OX2 6GG, United Kingdom
[d] Department of Mathematics, Imperial College London, London SW7 2AZ, United Kingdom
[e] Institut Jean le Rond ∂'Alembert, Sorbonne Université, CNRS, F-75005 Paris, France
[f] Department of Mechanical Engineering, University College London, London WC1E 7JE, United Kingdom

GRAPHICAL ABSTRACT

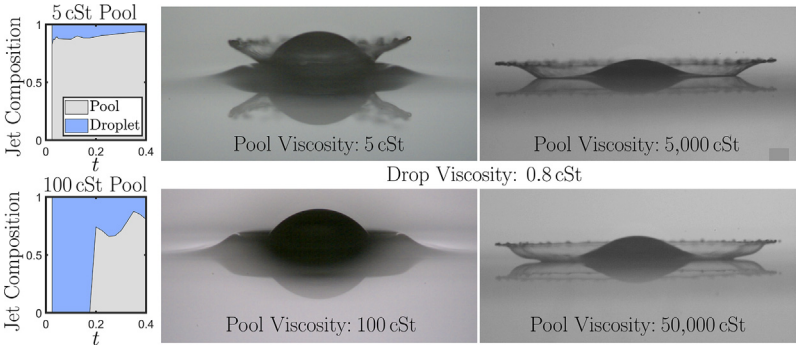

ARTICLE INFO

Article history:
Received 23 November 2022
Revised 14 February 2023
Accepted 5 March 2023
Available online 17 March 2023

Keywords:
Drops
Splashing
Wetting
Impact
Experiment
Direct numerical simulation

ABSTRACT

Droplet impact onto liquid pools is a canonical scenario relevant to numerous natural phenomena and industrial processes. However, despite their ubiquity, multi-fluid systems with the drop and pool consisting of different liquids are far less well understood. Our **hypothesis** is that the post-impact dynamics greatly depends on the pool-to-droplet viscosity ratio μ_p/μ_d, which we explore over a range of six orders of magnitude using a combination of **experiments** and **theoretical approaches** (mathematical modelling and direct numerical simulation). Our **findings** indicate that in this scenario the splashing threshold and the composition of the ejecta sheet are controlled by the viscosity ratio. We uncover that increasing the pool viscosity decreases the splashing threshold for high viscosity pools ($\mu_p/\mu_d \gtrsim 35$) when the splash comes from the droplet. By contrast, for low viscosity pools, the splash sheet comes from the pool and increasing the pool viscosity increases the splashing threshold. Surprisingly, there are conditions for which no splashing is observed under the conditions attainable in our laboratory. Furthermore, considering the interface velocity together with asymptotic arguments underlying the generation of the ejecta has allowed us to understand meaningful variations in the pressure during impact and rationalise the observed changes in the splashing threshold.

1. Introduction

Droplet impact onto a deep pool is a topic that has seen significant research owing to the plethora of phenomena for which it acts

* Corresponding author.
E-mail addresses: benjamin.fudge@eng.ox.ac.uk (B.D. Fudge), radu.cimpeanu@warwick.ac.uk (R. Cimpeanu), arnaud.antkowiak@upmc.fr (A. Antkowiak), castrejon@cantab.net (J.R. Castrejón-Pita), alfonso.castrejon-pita@wadham.ox.ac.uk (A.A. Castrejón-Pita).

https://doi.org/10.1016/j.jcis.2023.03.040
0021-9797/

as a fundamental framework. Examples include the formation of a Rayleigh jet and break-up into droplets [1–3], the formation and subsequent collapse of craters on impacts on a low viscosity pool [4–7], the entrapment of air bubbles [8,9], the formation of a sheet at the droplet-pool interface [10,11], the oblique impact of a droplet onto a pool [12,13] or impact and splashing on to moving liquid surfaces [14,15]. In most past scenarios, both the impacting drop and the pool are composed of the same liquid. In moderate-to–high speed scenarios, the focus has been on the complex early stages of impact, which culminate, in the more violent cases, in the formation of liquid sheets which are then subject to break-up. The combination of experimental and numerical tools [11] has enabled a more comprehensive understanding of the micromechanics of splashing, as it has given access to the intrinsic dynamics not visible by experiments alone. Moreover, it has led to rich mathematical models for the pressure variation during impact and the key velocities in the system [16,17,6,18]. Once such an early-time splashing structure is formed, the analytical framework of Wagner theory [19] provides asymptotic and complex analytical machinery that has been shown to be both powerful and informative within its regime of applicability [20]. Intricate dynamics has been observed and carefully studied at later stages of the impact as well, with cavity formation inside the pool being followed by the formation of a rapid vertical jet, which upon fragmentation leads to the ejection of secondary droplets [2,21]. By contrast, the impact of a droplet onto a different fluid provides challenges that require paradigm shifts from the single-fluid systems. The introduction of a distinct second liquid permits the variation of physical properties such as density and viscosity between the droplet and pool. Previous work in three-phase flows in the context of droplets has been concentrated on the dynamics of liquid lenses [22], for which numerical modelling has been attempted [23,24] and extended to the impact of droplets of different fluids for ‘cleaning’ applications [25]. Only very recently [26–28,18,29] has progress in two-liquid impact (in a surrounding gas) with significant variations in fluid properties been made experimentally and numerically (although a true three-phase flow was not incorporated numerically), revealing significant changes in the dynamics of the interfaces, the formation of the liquid sheet, and its shape and composition.

In the single-fluid impact regime, the splashing threshold is one of the most studied quantities due to its practical applications in the canonical scenario of drop impact onto flat surfaces, but also in moderate-to–high-speed impact onto rough surfaces [30], oblique impact [31–33], impact at reduced pressures [34] or onto soft solids [35]. Research into the splashing threshold for two-fluid impact is more limited however. For the case of droplet impact onto thin films of a different fluid, Kittel et al. [27] studied the splashing threshold in terms of the film to droplet viscosity ratio, and concluded that the dynamics is controlled by the properties of the lower viscosity fluid, as this is where splashing originates from. Marcotte et al. [28] examined ethanol droplet impact onto deep water-glycerol solution pools, which allowed the variation of viscosity in a miscible setup in which the interfacial tension was set to zero. The investigation focused on the impact process, interface shape identification and orientation changes of the ejected sheet upon impact. Unfortunately, the splashing threshold was not discussed, however the contributions of the different liquids to the ejected sheet as the viscosity ratio varied was discussed qualitatively therein. Knowledge of the relative proportion of liquids in multi-component droplets is of relevance in numerous applications [26,36], however the resulting configurations are challenging to either predict or measure in the absence of computational modelling or highly specialised image processing capabilities.

Despite this early progress, a comprehensive understanding of the effect of the liquid pool properties on splashing is still lacking. In this work we experimentally investigate the impact of a droplet onto a viscous pool across several orders of magnitude of viscosity ratios ($\mathcal{O}(1) - \mathcal{O}\left(1 \times 10^6\right)$) and quantify the effect of this ratio on the splashing threshold. This is complemented by high-resolution direct numerical simulation of three-phase impacts, looking at the jet composition as the viscosity ratio varies and its comparison with experimental observations. Finally, we theoretically develop a model for the splashing threshold using a combination of analytical arguments, numerical data, and the dynamics of the drop-pool interface extended from our previous work [18].

2. Experimental method

Our setup is illustrated in Fig. 1 (a) where drops of Fluorinert FC-770 were generated from a stainless steel needle and a syringe pump to fall under gravity. Droplets impact onto a 20 mm-deep pool filled with silicone oil, with viscosity μ_p ranging between $2 - 1,000,000$ cSt. Fluorinert is chemically stable, inert, resistant to contamination, and has a high density and low surface tension leading to splashing at low impact speeds. Silicone oils and FC-770 are immiscible, providing a factor scarcely investigated in liquid-on-liquid impacts. The impact events are captured with a high speed camera (either a Phantom v12 or a Phantom v2512) in a shadowgraphy configuration at up to 310,000 frames-per second and resolutions of $\sim 6\,\mu$m per pixel. The pool depth is large enough to prevent any boundary effects due to the finite-size of the container. The impact velocity is varied by adjusting the fall height. Silicone oils have constant density and surface tension over the viscosity range used here. Image analysis is used to obtain the droplet impact speed, diameter, eccentricity e (defined as $e = \sqrt{1 - b^2/a^2}$, where a and b are the major and minor semiaxes of the ellipse fitted to the droplet), and orientation. Only impacts with a low eccentricity ($e < 0.3$) are retained to avoid effects associated to shape irregularities [37]. Note that in upcoming sections we use the convention of the time of impact $t = 0$ ms being given by the first post-coalescence experimental frame observed in a typical series.

3. Direct numerical simulation

Direct numerical simulations are carried out using Basilisk [38–40] to provide greater insight into regions that are challenging to visualise. A three-phase setup is deployed to resolve the multi-fluid system consisting of the drop, the impacted pool and surrounding gas. This computational environment has been validated previously by Fudge et al. [18]. This method allows us to individually track each of the phases and thus study the splashing characteristics to quantify the effect of the viscosity ratio on the jet composition. Fig. 1 (b) shows the simulation setup. We use adaptive mesh refinement to vary the grid resolution on the regions of interest resulting in much more efficient simulations with a maximum resolution of $0.5\,\mu$m per grid point (~ 1860 grid points per diameter) with an example mesh shown in Fig. 1 (c). The length and velocity scales are made dimensionless using the droplet diameter D and impact velocity V_0 and the time scale is made dimensionless by D/V_0. The Fluorinert-air surface tension coefficient is denoted by σ_{da} (drop-air) and has a constant value $\sigma_{da} = 15.0 \pm 0.1\,\mathrm{mNm}^{-1}$, while the pool-air surface tension coefficient σ_{pa} is characterised by a value of $\sigma_{pa} = 20.0 \pm 0.1\,\mathrm{mNm}^{-1}$, as given by the used silicone oil-air properties. We note that the value for the interfacial tension coefficient between silicone oils and air varies by less than 5% across the viscosity range considered here. For the Fluorinert-silicone oil interface we experimentally measure

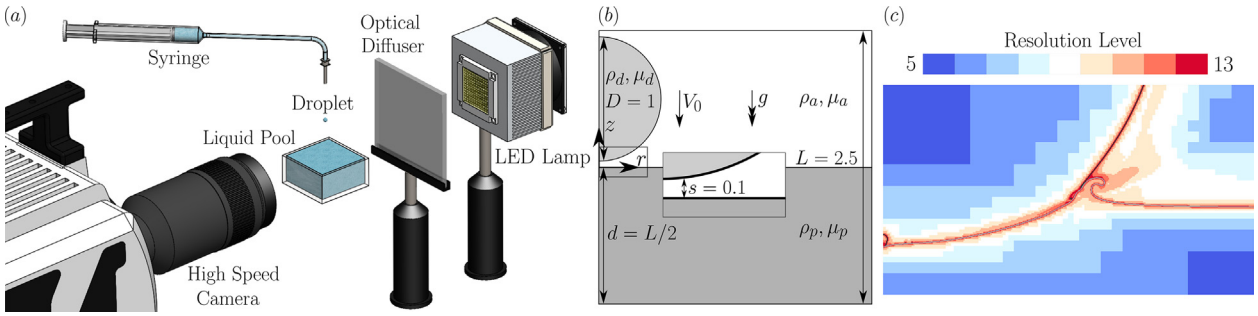

Fig. 1. (a) Diagram of the experimental setup, with a single camera capturing both the falling droplet and the subsequent post-impact dynamics. (b) Sketch of the axisymmetric simulation domain in its initial state. (c) Zoomed-in view for a typical simulation showing the adaptive mesh refinement, achieving spatial resolutions down to 0.5 μm.

the interfacial tension using the pendant drop method for several different oil viscosities, achieving a constant value of the drop-pool surface tension coefficient denoted σ_{dp} to be $\sigma_{dp} = 4.6 \pm 0.2\,\mathrm{mNm}^{-1}$, which we use for the simulations. Fig. 2 depicts example numerical interfaces for three different impact scenarios, revealing excellent agreement with experiments. In computational datasets $t = 0$ corresponds to the theoretical time of contact between the droplet and pool if neither deformed, a definition which has proven a robust counterpart to its experimental equivalent introduced at the end of Section 2.

The key quantitative outputs we consider are interfacial shapes, as well as information on velocities, viscous stresses, pressures, and vorticity that aid our understanding of the rich impact landscape. Moreover, using the three-phase method allows us to individually track, among many other properties, the contribution from each of the phases to the ejected jet and thus splashing characteristics, and therefore quantify the effect of the viscosity ratio on the jet composition: Resulting fluid–fluid interfaces are processed in order to extract the jet composition, as illustrated in Fig. 3 for two different impact scenarios. In each case the root of the jet is identified based on the two points of maximum curvature either side of the jet tip. The jet base is then taken as the straight line between these two points denoted by the dashed black line in Fig. 3. The total jet volume and the volumes of the pool and droplet within the jet are then found by integrating the profiles between the jet roots. This level of detail, alongside associated numerical information, allows us to expand on experimental findings and generate predictive capabilities, to be discussed in the following section.

4. Discussion

The impact outcome is shown in Fig. 4 in terms of the commonly used splashing parameter K when quantifying the splashing threshold [31,41–43] versus the pool-to-droplet viscosity ratio, $\mu_r = \mu_p/\mu_d$. Here $K = \mathrm{We}\sqrt{\mathrm{Re}} = \sqrt{\left(\rho_d^3 D^3 V_0^5\right)/(\sigma_{da}^2 \mu_d)}$, where $\mathrm{We} = \rho_d D V_0^2/\sigma_{da}$ and $\mathrm{Re} = \rho_d D V_0/\mu_d$ are the Weber and Reynolds numbers with $\rho_d, D, V_0, \sigma_{da}$ and μ_d denoting the droplet density, diameter, impact velocity, surface tension, and viscosity. We have considered the splashing threshold of K as the midpoint between

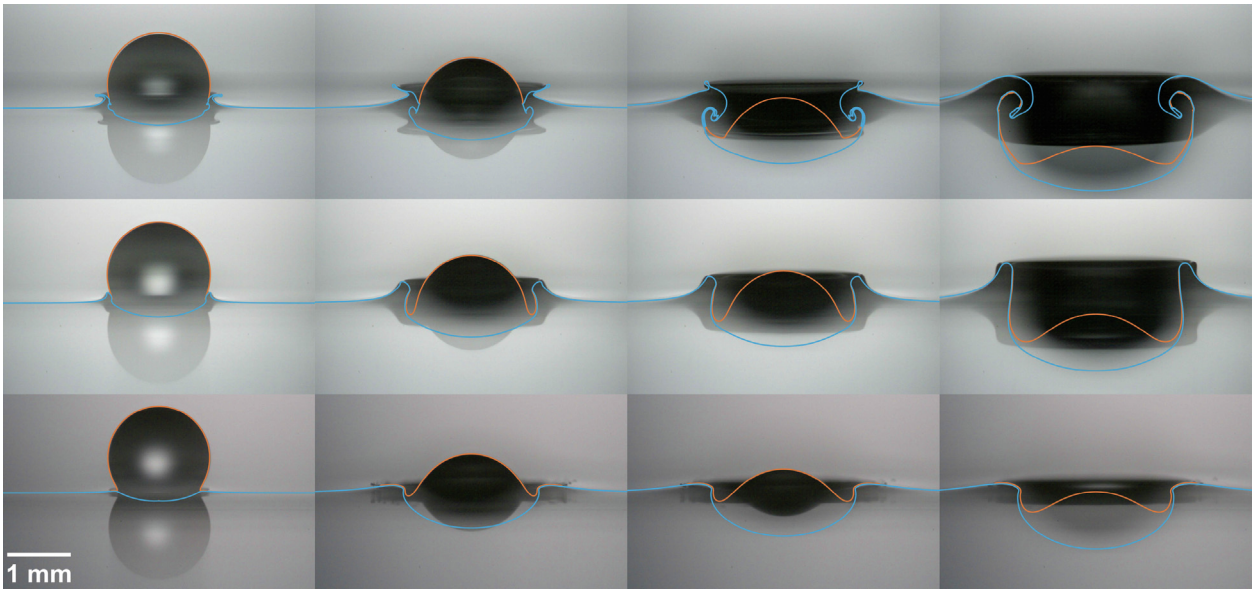

Fig. 2. Comparison between experimental data (background images) and direct numerical simulation results (highlighted coloured interface shapes) for the impact of 1.6 mm FC-770 droplets at 3.2 ms^{-1} onto: 20 cSt silicone oil pool at times 0.12 ms, 0.24 ms, 0.44 ms and 0.72 ms post-impact from left to right (top row), 50 cSt silicone oil pool at times 0.08 ms, 0.24 ms, 0.32 ms and 0.56 ms post-impact from left to right (middle row) and 350 cSt silicone oil pool at times 0.04 ms, 0.28 ms, 0.36 ms and 0.48 ms post-impact from left to right (bottom row). In each case the droplet interface in orange and pool interface in blue extracted from corresponding simulations are both overlaid on top of the experimental images. The scale bar in the bottom left frame applies throughout. Supplementary video material of direct numerical simulation data (fluid phases and adaptive grid) is included for each of the three examples.

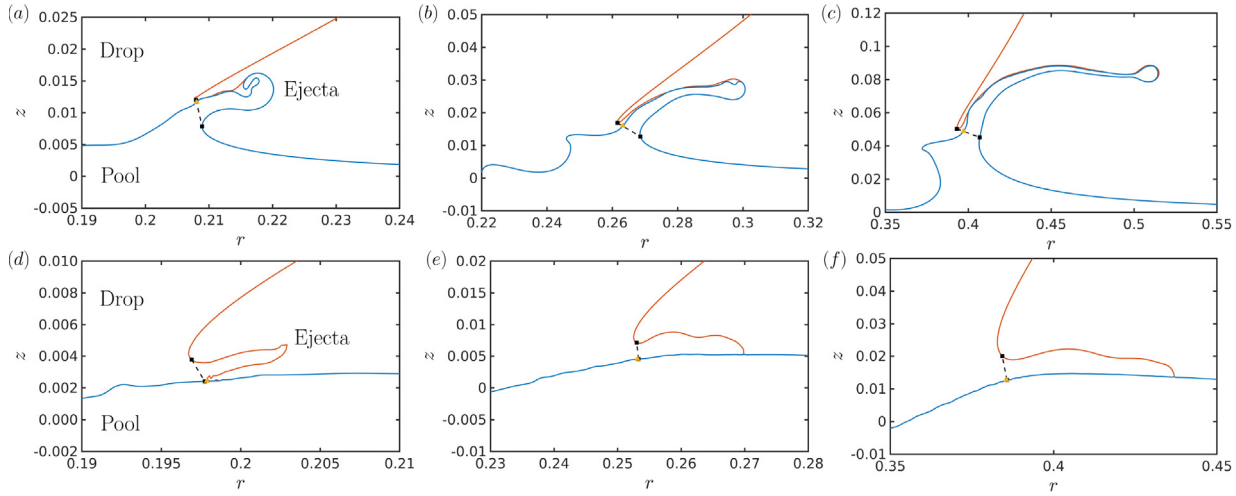

Fig. 3. Example calculation of jet contributions for the impact of a 1.6 mm FC-770 droplet at 3.2 ms^{-1} onto a pool with (a) $\mu_p = 5$ cSt at $t = 0.03$, (b) $\mu_p = 5$ cSt at $t = 0.05$, (c) $\mu_p = 5$ cSt at $t = 0.125$, (d) $\mu_p = 350$ cSt at $t = 0.03$, (e) $\mu_p = 350$ cSt at $t = 0.05$ and (f) $\mu_p = 350$ cSt at $t = 0.125$. In each case the droplet-air interface is illustrated in orange, and the pool-air interface is shown in blue (note that in some locations these overlap, with blue depicted on top as convention). The two jet root points of maximum curvature on either side of the jet tip are marked with black squares determining the endpoints for calculating the jet volume. The top and bottom rows correspond to the left and rightmost plots in Fig. 5, respectively. Note the different axis scales in each plot which are the dimensionless simulation radial position and height.

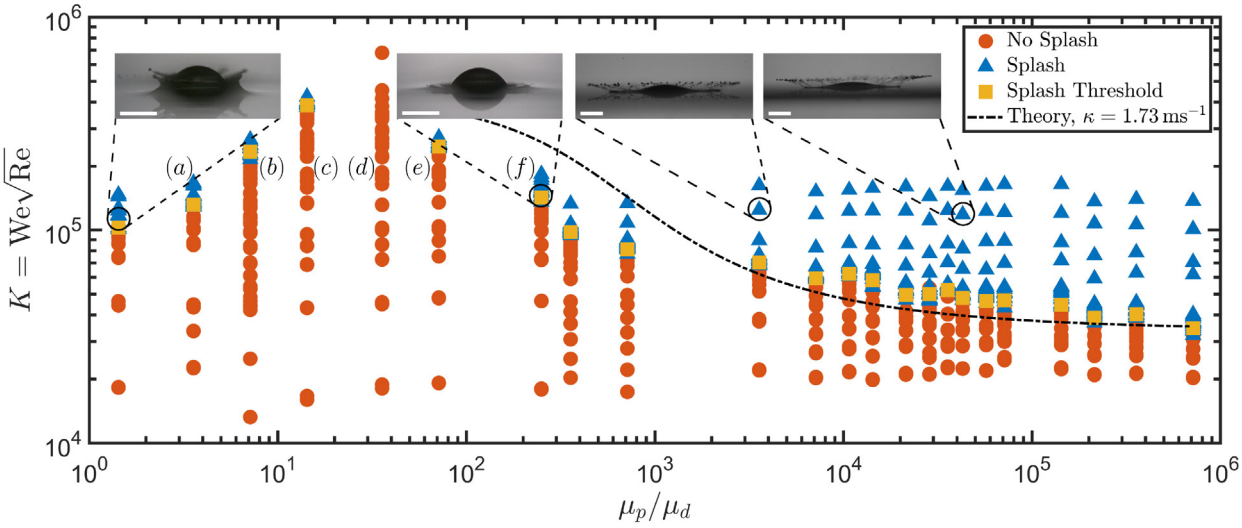

Fig. 4. Regime diagram summarising the impact behaviour characterised by the splashing parameter K versus the pool to droplet viscosity ratio, delineating impacts that splash (blue triangles) from those that don't (orange circles), as well as the splashing threshold (yellow squares). For the case of a viscosity ratio of ~ 35 no fall height available in the experimental setup resulted in splashing. The dot-dashed line corresponds to the solution to theoretical threshold from the solution of eq. (5) with a κ value of 1.73 ms^{-1}. The inset snapshots show examples of splashing at $K \sim 120,000$ for four different viscosity ratios with the scale bar in the bottom left corner being 1 mm in each case. Representative video supplementary material is also provided. The (a)-(f) labels correspond to the plots in Fig. 5. Note the logarithmic scale on both axes.

the splashing/non-splashing regions, denoting it as yellow squares in Fig. 4. The inset images show splashing for four different viscosity ratios (1.39, 242.75, 3467.86 and 41614.29) at an approximately constant K value of 120,000, which allows us to visualise the qualitative difference between the impacts at different pool viscosities. Specifically we observe that there is noticeable pool motion for the lower pool viscosity cases, whereas for the higher viscosities there is no significant deformation and the impact dynamics resembles that onto a solid. Also note that for the higher two of these viscosities the K value is significantly above the threshold, and thus the splash appears significantly more vigorous than for the two lower ratios.

Quantitatively we observe that, for low pool viscosity ratios ($\mu_p/\mu_d < 35$), the splashing threshold increases with pool viscosity. By contrast, for greater pool viscosities ($\mu_p/\mu_d > 35$) the threshold does the opposite. An intuitive explanation is that, as the pool viscosity increases, the pool motion decreases and thus less energy is removed from the droplet, making a splash more likely. At $\mu_p/\mu_d \sim 35$ ($\mu_p = 50$ cSt) no experimental condition resulted in splashing (our maximum impact speed was $V_0 = 5.62\,ms^{-1}$, or $K = 681,396$). Interestingly, a numerical investigation of this scenario also led to no evidence of splashing. In fact, simulations were performed at other higher velocities, up to the theoretical terminal velocity of the drop, and no liquid fragmentation was detected. We identify that $\mu_p = 50$ cSt marks the transition below which the ejected splash originates from the pool fluid (crown splash), whereas above this viscosity the splash comes from the droplet (prompt splash). Our hypothesis is that increasing the pool viscosity has opposing effects on the different types of splashing, i.e. increasing the pool viscosity inhibits crown splashing, but enhances

prompt splashing. Consequently we believe that this pool viscosity corresponds to the point where the overall splash suppression is the highest when considering a combination of the two mechanisms. This is consistent with the previous observation that the pool displacement is very small for higher viscosity pools, making it unlikely that the splash would come from it.

Next we turn our attention to a quantitative discussion of the jet composition and how this relates to which fluid contributes to the splash. We will also expand upon the discussion of the jet composition in [28] in view of the generalised setup herein. As noted in Section 3, the DNS platform allows us to extract the interfaces of the three different phases. This enables us to identify the jet region and the contribution of each fluid to it, as illustrated in Fig. 3. We perform a systematic investigation of the jet composition across several different pool viscosities as a function of time during the impact process. We restrict ourselves to pool viscosities of up to 350 cSt (corresponding to a pool to droplet viscosity ratio of 242.75), given the already large scale physical property contrast between the pool and surrounding gas, encompassing between them several orders of magnitude in this key parameter. We note however that from the experimental videos we can see that above this viscosity there is no significant phenomenological change in the impact process. Consequently we now limit ourselves to pool viscosities within the range $5-350$ cSt, as denoted by the points (a)-(f) in Fig. 4. In each case the impact is characterised by a K value of $165,000$. We present these results in Fig. 5, where we plot the percentage of the jet from each of the fluids (pool and droplet) against the simulation time for several pool viscosities. At this stage it is useful to recall the definition of the jet root as being identified by two points of maximum curvature either side of the jet tip, also previously highlighted in Fig. 3. The white area at early times in all cases corresponds to the time before which the jet has formed (which is a largely constant value across all of the viscosities).

From the plot we can see the clear trend that as the viscosity ratio increases, a progressively larger proportion of the jet originates from the droplet compared to the pool. This agrees with our earlier observation and intuition that a more viscous pool will deform less prominently and thus contribute less fluid into the jet. We notice that for the 5, 10 and 20 cSt viscosity pools the jet is almost entirely composed by fluid coming from the pool across all times. By contrast, for 50 and 100 cSt viscosity pools we identify a transition in which at early times the jet is entirely composed of droplet fluid, but then at later times contributions from the pool also begin to materialise. Comparing the 50 and 100 cSt pool viscosity cases we can see that this transition happens at a later time and with a smaller amount of pool liquid inside the jet. Finally, we find that when the pool viscosity is 350 cSt, the jet contains only fluid from the droplet, with the impact region acting more similar to a (weakly) compliant solid. The plots in Fig. 3 shed more light into the morphological features of the interfaces during this dynamics. The top row corresponds to the 5 cSt pool, where we can see that the droplet contributes to the upper portion of the jet, with significant deformation of the pool. The bottom row illustrates the 350 cSt pool, where we only observe a slight rising of the pool surface at the location of the jet root but the dynamics itself consists simply of a droplet spreading on the pool surface. This indicates good qualitative agreement to the results of Marcotte et al. [28], who show similar simulation profiles in their Fig. 2.

Our earlier experimental observation on the source of the splash coming from the pool for $\mu_p/\mu_d < 35$ and from the droplet for $\mu_p/\mu_d > 35$ is thus reinforced by the above analysis and cross-comparison between experimental and numerical findings, as well as recent results from the literature. In what follows we aim to provide a mechanistic explanation of the above, providing predictive capabilities beyond the specific parameter regimes discussed previously.

5. Theoretical approach

We now provide a theoretical model for the two different splashing threshold trends identified in Section 4 and attempt to derive models quantifying them. We consider both the high viscosity region ($\mu_p/\mu_d > 35$) where the splash comes from the droplet and the threshold to splash decreases with pool viscosity, as well as the low viscosity region ($\mu_p/\mu_d < 35$) where the splash comes from the pool and the threshold to splash increases with pool viscosity, as they are phenomenologically unique.

First we consider the high viscosity case, which shares similarities to the scenario in which the threshold to splash on a soft solid decreases as the solid becomes more firm [35]. Following Howland et al. [35], we explain this by first noting that as the pool viscosity increases the displacement decreases and the peak pressure in the droplet increases. Fig. 6 shows the peak pressure inside the droplet as a function of time for simulated impact scenarios with a constant K value of $165,000$ and for several different pool viscosities. From the figure we identify the overall trend that increasing the pool viscosity increases the peak pressure in the droplet, as well as the maximum value in time of this maximum pressure. At the time of impact the maximum pressure occurs at the centerline, but it quickly moves off-axis to follow the contact line as the impact proceeds further and the droplet spreads out. Near the contact line, the pressure continues to increase until the jet is formed,

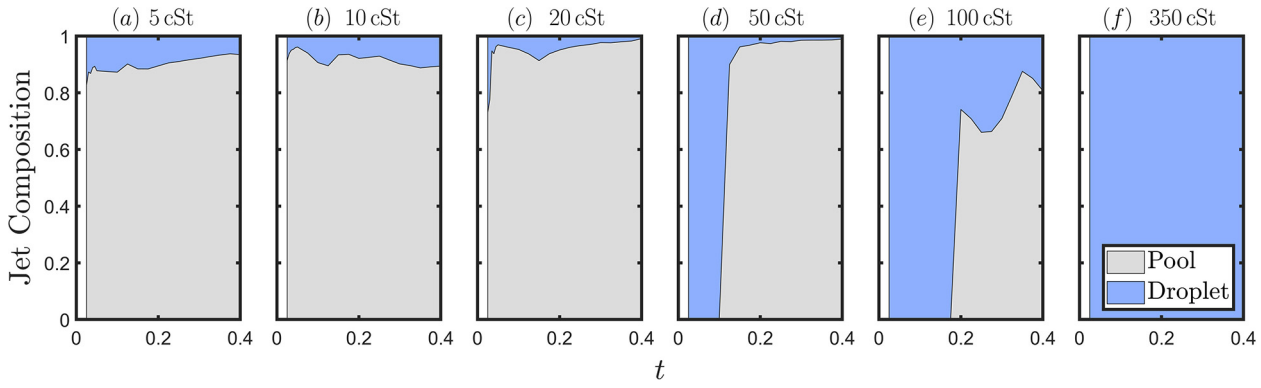

Fig. 5. Post-impact jet composition versus time for impact cases described by $K = 165,000$ onto pools characterised by viscosities of $5, 10, 20, 50, 100$ and 350 cSt, respectively. Here $t = 0$ corresponds to the theoretical time of impact if neither the pool nor the droplet were to deform pre-impact. The white area at early times in each case depicts the time interval during which the jet has not yet formed.

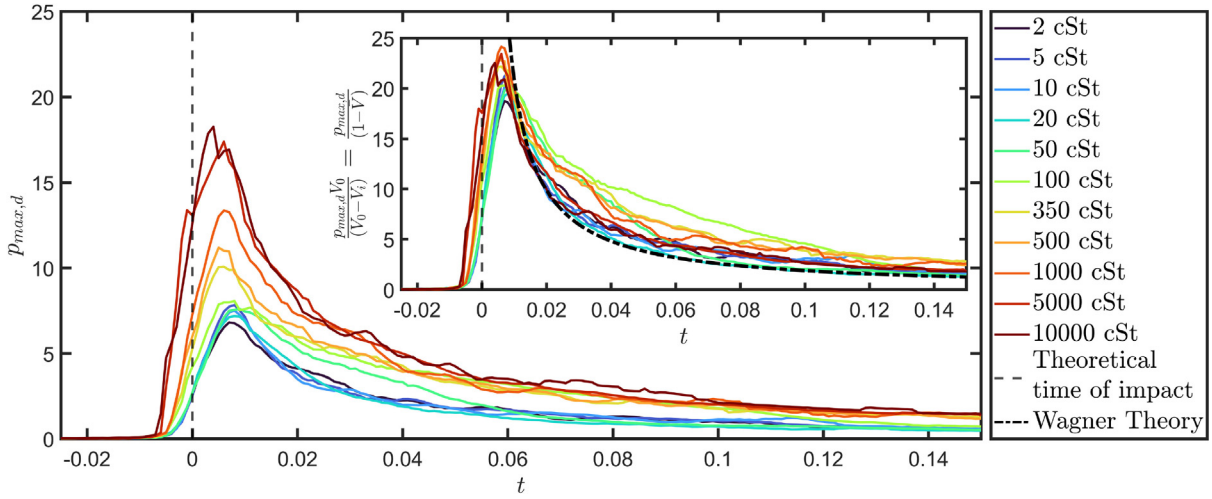

Fig. 6. Droplet peak pressure against time for several different pool viscosities (direct numerical simulation data). In each case the key impact parameter is $K = 165,000$ and $t = 0$ corresponds to the theoretical time of impact if neither droplet nor pool deformed. (Inset) The same pressure is normalised by $\frac{V_0}{(V_0-V_i)} = \frac{1}{(1-\bar{V})}$, where V_i is the velocity of the common droplet-pool interface [18].

and then decreases thereafter. This holds for both high viscosity pools where the jet is formed with fluid from the droplet and low viscosity pools where the pool is the main contributor to the jet composition. Fig. 7 (a) illustrates experimental snapshots revealing the faster spreading of the jet for higher viscosity pools, which is consistent with the hypothesis that the pool deformation reduces the pressure driving the jet, causing it to form more slowly as the pool deformation is enhanced at lower viscosities.

A significant feature is that for pool viscosities of less than 100 cSt there is little variation in the peak droplet pressure with viscosity, but above this viscosity value we begin identifying noticeable increases in the peak droplet pressure with larger pool viscosities. As this viscosity of 100 cSt corresponds to the region in our parameter space where splashing from the droplet is observed, we believe therefore that this corresponds to the threshold peak pressure in the droplet that must be exceeded in order for prompt splashing to occur. Using several helpful mathematical building blocks, we are for the first time in a position to elucidate this process in detail. We begin by providing an explanation for the reduction in the peak pressure. As noted by Howland et al. [35], we can use arguments stemming from Wagner theory [19] for liquid impact to probe the structure of the pressure field in the droplet. This theory, originally designed to describe the stresses exerted on a solid object impacting a body of liquid, can equally be well used to infer the pressure field in a drop impacting a solid substrate [e.g. 44]. A detailed theoretical analysis of the pressure field near the contact line [45,46] reveals that the maximum pressure simply reads $\rho_d \dot{a}^2/2$, where $a(t) = \sqrt{3RV_0(t - t_{\text{impact}})}$ is the location of the contact line [35] as demonstrated in Fig. 7 (b). As a result, the peak pressure in the droplet is given by

$$p_{\text{max,d}}^{\text{Wagner}} = \frac{3\rho_d R V_0}{8\delta t}, \tag{1}$$

where δt is the of time between sheet ejection (when the pressure reaches a maximum) and theoretical impact if neither droplet or pool deformed.

The argument above is justified by considering Fig. 7 (b), specifically the inset, in which we depict the early time motion of the jet as being very well predicted by the use of Wagner theory estimates within their expected range of applicability. We note however that this result originally comes from impact onto a solid – and static – surface. Therefore we transform it into the velocity that the droplet actually experiences as $V_0 - V_i$, where V_i is the speed of the droplet-pool interface, which is the relative velocity of the droplet into the pool. Consequently we can rewrite Eq. (1) for impact onto liquid pools as Eq. (2), where we now use the velocity of the droplet relative to the pool. From this equation we expect a reduction

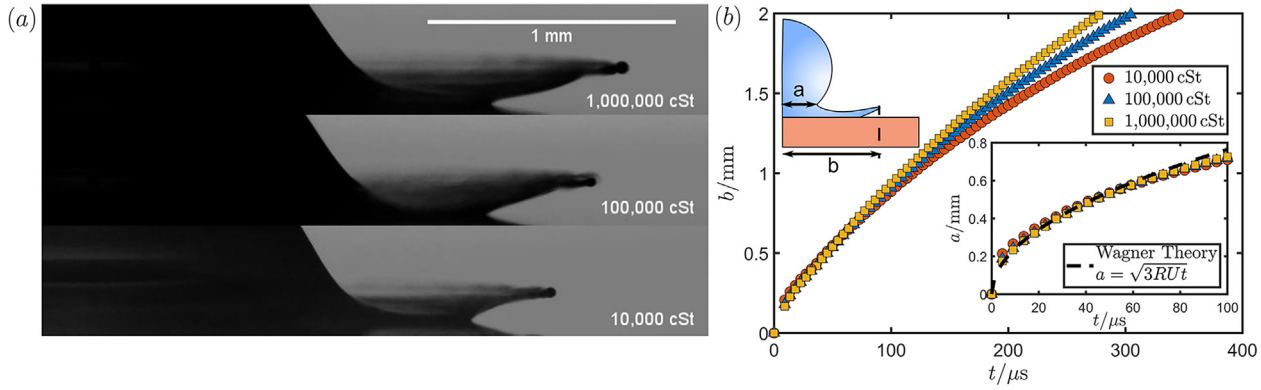

Fig. 7. (a) Snapshots of 1.6 mm diameter FC-770 droplets impacting onto silicone oil pools at 2.5 ms^{-1}, taken at 300 μs post-impact (video supplementary material also included). (b) Measurement of the spreading distance of the tip of the jet (main figure) and the root of the jet (lower inset) as defined in the upper inset. In the case of the jet root location the result predicted by Wagner theory is also included.

in the maximum droplet pressure for less viscous pools due to V_i being larger, which is consistent with the results in Fig. 6, and is expressed as

$$p_{\max,d} = \frac{3\rho_d R(V_0 - V_i)}{8\delta t} = \frac{V_0 - V_i}{V_0} p_{\max,d}^{\text{Wagner}}. \tag{2}$$

In order to determine this relative velocity we use the result derived by Fudge et al. [18] to find the pool velocity, resulting in $V_0 - V_i = V_0(1 - \overline{V})$, where $\overline{V} = V_i/V_0$ is the normalised common interface penetration velocity given by

$$\overline{V} = \frac{V_i}{V_0} = \frac{1}{\sqrt{1 + A\rho_r + \frac{C}{\mathrm{Re}_d}\mu_r}}, \tag{3}$$

where the parameters A and C have values of 2.7096 and 24.3984, respectively. Fig. 8 (a) illustrates the predictions obtained via eq. (3) extended to much higher viscosity ratios than previously explored in [18], as well as penetration velocities extracted from simulations and experiments indicating that the model remains valid even at these higher viscosities justifying its use here. Encouraged by the observed robustness of this prediction, if we normalise the measured maximum pressure by dividing through by $\frac{V_0 - V_i}{V_0}$ in Eq. (2) we should recover the Wagner maximum pressure, which we would no longer anticipate to vary with viscosity. In the inset of Fig. 6 we can visualise the normalised droplet maximum pressure versus time, showing a very good collapse of the curves across all values of the pool viscosity, as well as good agreement with the theoretical result predicted by Wagner theory (dash-dotted lines).

The pressure estimate (2) above may also be used to explain the decrease in the splashing threshold for high pool viscosities. As in Howland et al. [35], we ascertain that for splashing to occur we require the maximum pressure in the droplet to exceed a threshold value, p_T. For splashing we therefore require $p_{\max,d} \gtrsim p_T$ and, using eq. (2), the expression for the maximum Wagner pressure in Eq. (1) and the equation for the common interface velocity in Eq. (3), leads to

$$V_{0,T} - V_i = V_{0,T}(1 - \overline{V}) \gtrsim \frac{8p_T\delta t}{3\rho_d R}, \tag{4}$$

where $V_{0,T}$ denotes the threshold droplet impact velocity to splash. Eq. (4) indicates that in order to splash we require the droplet impact velocity relative to the pool to exceed a threshold value given by $\frac{8p_T\delta t}{3\rho_d R}$, which we hereafter denote as κ. This is consistent with impact onto a solid surface, where V_i would be zero, and we would simply require the droplet impact speed to exceed a given threshold. We note that in eq. (4) the right hand side is a constant and the left hand side depends on the droplet impact speed and pool viscosity (via $\overline{V}$). We can therefore use this equation to find the threshold impact speed to splash for a given viscosity ratio. Substituting in the equation for the penetration velocity (3), algebraic manipulation leads us to the inequality

$$V_{0,T}^3[\rho_d D(A^* - 1)] + V_{0,T}^2(C\mu_d\mu_r - 2\kappa\rho_d DA^*) + V_{0,T}(\kappa^2\rho_d DA^* - 2\kappa C\mu_d\mu_r) + \kappa^2 C\mu_d\mu_r \gtrsim 0, \tag{5}$$

where $A^* = 1 + A\rho_r$ and C originate from the penetration velocity given by eq. (3), μ_d is the droplet viscosity, μ_r the pool to droplet viscosity ratio and κ is the required excess speed as above. The selection of the correct root in the cubic equation relies, in first instance, on excluding the one (non-physical) negative root arising within our parameter space. Differentiating between the two remaining positive values is then supported by physical arguments, with the larger of the two roots decreasing in value as the pool viscosity increases being consistent with experimental data.

If we briefly consider the distinguished limit scenario of the pool viscosity tending to infinity, we recover the equation $V_{0,T}^2 - 2\kappa V_{0,T} + \kappa^2 \gtrsim 0$, which has the solution of $V_{0,T} > \kappa$, as we expected above. In order to use this equation we need a value of κ and therefore require estimates for the threshold pressure to splash and the time of sheet ejection. For the threshold pressure we can use the result by Howland et al. [35] and note that a pressure of 93 kPa was consistent with their findings and also with the pressures in the droplet measured in this work obtained by dimensionalising the data in Fig. 6. To retrieve the jet ejection time we performed experiments and found a consistent value of $\sim 30\,\mu$s across several pool viscosities, again consistent with the framework of impact onto soft solids [35]. We do note however that using these values for p_T and δt leads to κ of $\sim 5\,\mathrm{ms}^{-1}$, which is far larger than the expected threshold speed for impact onto a solid surface. One possible explanation for this discrepancy is that the small time interval describing these dynamics in the experiments at these high speeds (approximately seven frames) makes the accurate determination of the impact time and first appearance of the sheet very challenging. This is exacerbated by the region of interest being obscured by the bulk of the droplet and pool (due to the intrinsic three-dimensional geometry of the interfaces), meaning that this value of $\sim 30\,\mu$s is thus more likely to be

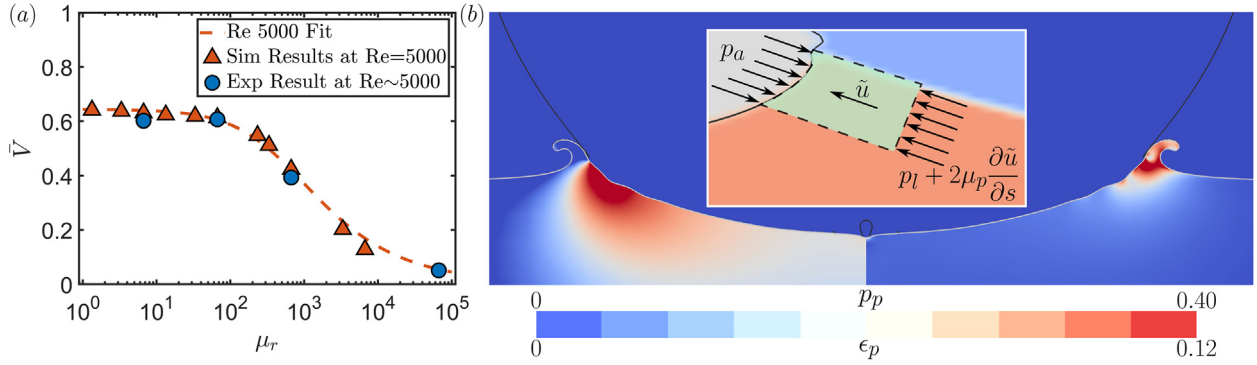

Fig. 8. (a) Droplet-pool interface velocity versus the pool to droplet viscosity ratio for an impact with Re = 5000, showing both simulation and experimental results which validate the use of the theoretical prediction from eq. (3) in this higher viscosity regime (the viscosity range is considerably extended from that in [18]). (b) Pool pressure (left hand side) and viscous stress (right hand side) for the case of the impact of a FC-770 droplet impacting onto a 20 cSt silicone oil pool at Re = 6660 and $t = 0.1$ dimensionless time post-impact, showing that the peak pressure and viscous dissipation are both concentrated at the root of the jet. The inset highlights the region around the jet root before its formation, showing the direction of the jet forming velocity $\tilde{u}$ as described in the main text, as well as a control volume (in green) showing the forces acting on it (where the subscripts a and l refer to the air and liquid respectively). Note here the colouring simply distinguishes the different phases. Note that illustrated quantities have been restricted to the pool for visual emphasis, and also the different (non-dimensional) scales for the two measures.

considered an upper bound on the possible ejection time. Comparing to the data-rich simulations however, we observe a much smaller time to ejection of $\sim 10\,\mu s$, resulting in an excess speed of $1.73\,ms^{-1}$, a value much closer to the observed splashing threshold for impact onto a solid surface which we find as $\sim 1.55\,ms^{-1}$ for the Fluorinert droplets used here. Fig. 4 includes the result of this theoretical argument with an excess speed of $1.73\,ms^{-1}$, indicating very good agreement with the data especially at higher pool viscosities. The observed difference at lower pool viscosities could be attributed to the droplet-pool interface not immediately reaching the (now higher) penetration velocity. Thus the motion of the common interface is actually slower and so the pressure damping is slightly less than predicted, resulting in an overestimation of the splashing threshold in this region of the parameter space.

We now focus further on the low pool viscosity section of the parameter regime, where we see splashing from the pool with an increase in the splashing threshold as the pool viscosity increases. As previously noted, Fig. 6 illustrates how for low pool viscosities the peak pressure in the droplet upon impact is largely unchanged (see variations up to 100 cSt) and thus it will not have an effect in this case. Therefore we turn our attention to the pressure inside the pool and how it affects the splashing behaviour. Firstly we underline that, based on experimental observation and analysis, the pool splashing is predicated on the formation of a jet (largely of pool fluid for low viscosities as shown in Fig. 5) from which the splash derives. From our experiments and simulations we can see that as the pool viscosity increases the jet becomes thicker and slower, and is therefore less likely to pinch off and eject a droplet (i.e. splash), which qualitatively explains why increasing the pool viscosity makes splashing less likely. We therefore concentrate in understanding the mechanism underlying the formation of this jet and in particular how it depends on the pool viscosity. As presented on the left hand side of Fig. 8 (b), similar to the maximum pressure in the droplet occurring at the root of the jet, the maximum pressure in the pool also occurs at the root of the jet and it is this pressure which is driving the jet formation. We also note that, as is the case in the droplet, the value of the maximum pressure inside the pool does not vary significantly for pool viscosities less than 100 cSt which is demonstrated in Fig. 9 (a). Thus the driving force behind the jet production is largely constant in this case and it must be the opposing force that is varying with the pool viscosity.

We consider the force opposing the jet formation to be the viscous stress, and approximate it as $2\mu_p \frac{\partial \tilde{u}}{\partial s}$, where $\tilde{u}$, shown in the inset in Fig. 8 (b), is the velocity in the direction of the jet formation s. As before, we assume that due to the largely constant penetration velocity in relation to changes in pool viscosity, this derivative should also be largely constant when considering different pool viscosity impact scenarios. We also note that this derivative has a negative value and thus the force from the viscous stress will be, as expected, acting in the negative s direction (i.e. in the opposite direction to the arrow in the inset in Fig. 8 (b)). Thus we hypothesise that the viscous stress varies linearly with the pool viscosity, an observation that is consistent with the data in Fig. 9 (b). This explains why the splashing threshold increases as the pool viscosity increases in this regime as the force driving the splash is largely constant, whereas the one opposing it is increasing (largely linearly) with the pool viscosity. We also observe that the maximum viscous stress occurs at the root of the jet, mirroring the position of the peak pressure inside the pool (right hand side of Fig. 8 (b)). This leads to the condition of a jet needing to form in order to support the splashing mechanism, for which we require the peak pressure in the pool to exceed the peak viscous stress. Fig. 9 (c) shows the ratio of the peak pressure to stress from which we identify that for the lower pool viscosities the peak pressure is consistently greater than the viscous stress. By contrast, for pool viscosities $\gtrsim 50$ cSt the peak pressure is largely less than the viscous stress, cases for which we do not see a formation of a pool jet.

These results verify our conjecture that the increase in the splash threshold for low pool viscosities is due to the increase in the viscous stress in the pool at the root of the jet, impeding its formation and slowing it down leading to a decreased tendency to splash. The simulation results indicate that the viscous stress starts to exceed the maximum pressure at a pool viscosity of approximately 50 cSt, which is when we no longer observe crown splashing from the pool in the experimental data.

Combined with the above results for the high viscosity pool cases, we have explained the observed trends in the splashing threshold across all the tested pool viscosities. Furthermore, by using the prediction for the velocity of the droplet-pool interface [18], we have quantified the effect of the pool motion and how the splashing threshold thus varies.

6. Concluding remarks

We have systematically examined the immiscible impact of liquid droplets onto deep viscous pools across several orders of magnitude of viscosity ratio. Both imaging and computational

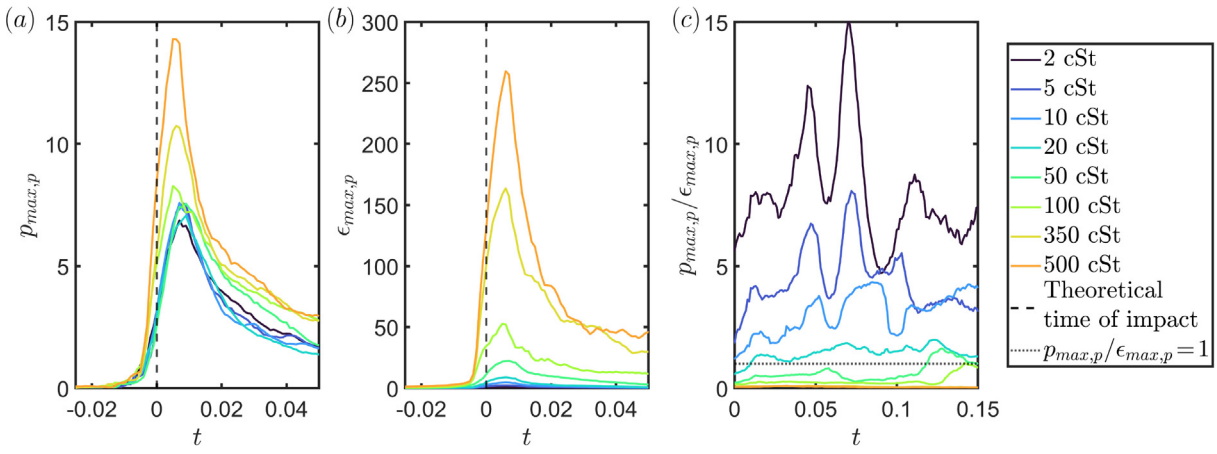

Fig. 9. Numerically obtained (a) peak pressure and (b) viscous stress inside the pool versus time for several different pool viscosities. (c) The ratio of the peak pressure to the viscous stress, noting that for jet formation we expect this ratio to be greater than unity (marked by a dotted line). In each case the impact is characterised by a splashing parameter $K = 165,000$, and $t = 0$ corresponds to the theoretical time of impact if neither droplet nor pool deformed. These points consist of a subset of those in Fig. 6 with a consistent colour scheme. Note the different scale on the y-axes.

capabilities required to conduct rigorous studies for multi-fluid impingement scenarios have only been developed in recent years, inspired by the need to understand natural phenomena and industrial applications such as environmental disaster mitigation after oil spills [26,47] or inkjet printing [36,48,49]. Drop impact onto immiscible liquid layers is a topic that has attracted recent interest [3,8], however, these works have been limited to describing phenomenological aspects of the problem, providing important but limited explanations regarding the underlying physical mechanisms controlling the post-impact dynamics. Thus far, efforts have been concentrated either on gentler, often capillary-dominated interfacial flow regimes [50–52], or in simplified fluid property formulation contexts [28]. The present study represents a first comprehensive incursion into a previously inaccessible and rich parameter regime. From this investigation we have observed a non-monotonic response of the splashing threshold against the viscosity ratio. For low viscosity ratios ($\mu_p/\mu_d < 35$) increasing the pool viscosity increases the threshold to splash, and in these cases the main contribution to the ejected liquid sheet originates from the pool. For higher viscosity ratios ($\mu_p/\mu_d > 35$) increasing the pool viscosity decreases the splashing threshold, and in these cases the splash sheets originate from the droplet, consistent with recent studies [27,28]. Interestingly, for a narrow intermediate regime found at $\mu_p/\mu_d \approx 35$, no splashing could be observed under conditions attainable in our laboratory, nor in our computational campaign. A specialised direct numerical simulation implementation has strengthened our experimental investigations, providing further insight into the underlying motion of both fluids. From these numerical results we have quantified how the different fluids contribute to the jet composition, and therefore the splash, across different velocities, allowing us to interpret the observed experimental results. We have quantified the resulting liquid jet composition in detail, with impact onto low pool viscosities leading to jets consisting mostly of pool fluid ($\approx 80-90\%$ for $\mu_p/\mu_d < 35$), while impact onto high pool viscosities can lead to the jet being entirely composed of fluid coming from the droplet. We also explained the cause for the decrease in splash threshold for high pool viscosities through a mechanism extending the arguments of Howland et al. [35]. Using a rigorous asymptotic approach aided by detailed numerical data, we found that the pool deformation at lower pool viscosities causes a reduction in the maximum pressure in the droplet, suppressing the splash. Using recent results by Fudge et al. [18] has allowed us to quantify this reduction and provide a compact and readily employable theoretical framework which has proven remarkably robust over large sections of the parameter space in this multi-fluid system. The resulting cross-methodological approach has generated new predictive capabilities not only in assessing primary impact features in vast three-phase flow parametric settings, but also in providing insight into splash sheet formation and eventual break-up into secondary droplets, all of key importance in the context of technological applications. Further extensions over sufficiently long timescales will likely require the incorporation of additional physics, such as thermal variation and Marangoni effects [53], particularly in scenarios involving lower speed impacts and where temperature gradients between drop and targets exist, or where miscible liquids are used. Opportunities to study late-stage dynamics involving cavity formation, as well as jet ejection and break-up [29] also become viable next objectives for investigation.

Declaration of competing interest

The authors declare that they have no known competing financial interests or personal relationships that would have influenced the body of work reported in this submission.

Funding acknowledgement

AACP thanks the Royal Society support through the University Research Fellowship (Grant No. URF|R|180016) & Enhancement Award (Grant No. RGF|EA|181002). RC and AACP gratefully acknowledge funding support from NSF/CBET-EPSRC grant EP/W016036/1. BF was supported by a Doctoral Training Award at the University of Oxford. For the purpose of Open Access, the author has applied a CC BY public copyright licence to any Author Accepted Manuscript (AAM) version arising from this submission.

Data availability

The direct numerical simulation implementation supporting the findings reported in this manuscript is openly available as part of the the GitHub repository at https://github.com/rcsc-group/DropImpactViscousPool.

Declaration of Competing Interest

The authors declare that they have no known competing financial interests or personal relationships that could have appeared to influence the work reported in this paper.

Appendix A. Supplementary material

Supplementary data associated with this article can be found, in the online version, at https://doi.org/10.1016/j.jcis.2023.03.040.

References

[1] E. Castillo-Orozco, A. Davanlou, P.K. Choudhury, R. Kumar, Droplet impact on deep liquid pools: Rayleigh jet to formation of secondary droplets, Phys. Rev. E 92 (5) (2015) 053022.
[2] S.K. Das, A. Dalal, M. Breuer, G. Biswas, Evolution of jets during drop impact on a deep liquid pool, Phys. Fluids 34 (2) (2022) 022110.
[3] Z. Che, O.K. Matar, Impact of droplets on immiscible liquid films, Soft Matter 14 (9) (2018) 1540–1551.
[4] U. Jain, M. Jalaal, D. Lohse, D. Van Der Meer, Deep pool water-impacts of viscous oil droplets, Soft Matter 15 (23) (2019) 4629–4638.
[5] H. Lhuissier, C. Sun, A. Prosperetti, D. Lohse, Drop fragmentation at impact onto a bath of an immiscible liquid, Phys. Rev. Lett. 110 (26) (2013) 264503.
[6] G.-J. Michon, C. Josserand, T. Séon, Jet dynamics post drop impact on a deep pool, Physical Review Fluids 2 (2) (2017) 023601.
[7] V. Lherm, R. Deguen, T. Alboussière, M. Landeau, Rayleigh–taylor instability in impact cratering experiments, Journal of Fluid Mechanics 937.
[8] D. Roy, S.S. Rao, S. Basu, Droplet impact on immiscible liquid pool: Multi-scale dynamics of entrapped air cushion at short timescales, Phys. Fluids 34 (5) (2022) 052004.
[9] T. Tran, H. de Maleprade, C. Sun, D. Lohse, Air entrainment during impact of droplets on liquid surfaces, J. Fluid Mech. 726.
[10] L. Zhang, J. Toole, K. Fezzaa, R. Deegan, Evolution of the ejecta sheet from the impact of a drop with a deep pool, J. Fluid Mech. 690 (2012) 5–15.
[11] M.-J. Thoraval, K. Takehara, T.G. Etoh, S. Popinet, P. Ray, C. Josserand, S. Zaleski, S.T. Thoroddsen, von kármán vortex street within an impacting drop, Phys. Rev. Lett. 108 (26) (2012) 264506.
[12] S.A. Reijers, B. Liu, D. Lohse, H. Gelderblom, Oblique droplet impact onto a deep liquid pool, arXiv preprint arXiv:1903.08978.
[13] M.V. Gielen, P. Sleutel, J. Benschop, M. Riepen, V. Voronina, C.W. Visser, D. Lohse, J.H. Snoeijer, M. Versluis, H. Gelderblom, Oblique drop impact onto a deep liquid pool, Physical Review Fluids 2 (8) (2017) 083602.
[14] J.R. Castrejón-Pita, B.N. Muñoz-Sánchez, I.M. Hutchings, A.A. Castrejón-Pita, Droplet impact onto moving liquids 809 (2016) 716–725.
[15] Z. Che, A. Deygas, O.K. Matar, Impact of droplets on inclined flowing liquid films 92 (2) (2015) 023032.
[16] C. Josserand, S. Zaleski, Droplet splashing on a thin liquid film, Phys. Fluids 15 (6) (2003) 1650–1657.
[17] C. Josserand, P. Ray, S. Zaleski, Droplet impact on a thin liquid film: anatomy of the splash, J. Fluid Mech. 802 (2016) 775–805.
[18] B.D. Fudge, R. Cimpeanu, A.A. Castrejón-Pita, Dipping into a new pool: The interface dynamics of drops impacting onto a different liquid, Phys. Rev. E 104 (6) (2021) 065102.
[19] H. Wagner, Über stoß-und gleitvorgänge an der oberfläche von flüssigkeiten, ZAMM-Journal of Applied Mathematics and Mechanics/Zeitschrift für Angewandte Mathematik und Mechanik 12 (4) (1932) 193–215.

[20] R. Cimpeanu, M. Moore, Early-time jet formation in liquid–liquid impact problems: theory and simulations, J. Fluid Mech. 856 (2018) 764–796.
[21] A. Singh, P. Kumar, Droplet impact dynamics onto a deep liquid pool of wavy free surface, Phys. Fluids 34 (2) (2022) 022107.
[22] C.G. Lyons, Lxxxiii.–the angles of floating lenses, Journal of the Chemical Society (Resumed) (1930) 623–634.
[23] F. Yeganehdoust, R. Attarzadeh, I. Karimfazli, A. Dolatabadi, A numerical analysis of air entrapment during droplet impact on an immiscible liquid film, Int. J. Multiph. Flow 124 (2020) 103175.
[24] B. Wang, C. Wang, Y. Yu, X. Chen, Spreading and penetration of a micro-sized water droplet impacting onto oil layers, Phys. Fluids 32 (1) (2020) 012003.
[25] O. Ramírez-Soto, V. Sanjay, D. Lohse, J.T. Pham, D. Vollmer, Lifting a sessile oil drop from a superamphiphobic surface with an impacting one, Science advances 6 (34) (2020) eaba4330.
[26] D.W. Murphy, C. Li, V. d'Albignac, D. Morra, J. Katz, Splash behaviour and oily marine aerosol production by raindrops impacting oil slicks, J. Fluid Mech. 780 (2015) 536–577.
[27] H.M. Kittel, I.V. Roisman, C. Tropea, Splash of a drop impacting onto a solid substrate wetted by a thin film of another liquid, Physical Review Fluids 3 (7) (2018) 073601.
[28] F. Marcotte, G.-J. Michon, T. Séon, C. Josserand, Ejecta, corolla, and splashes from drop impacts on viscous fluids, Phys. Rev. Lett. 122 (1) (2019) 014501.
[29] F. Minami, K. Hasegawa, Cavity and jet formation after immiscible droplet impact into deep water pool, Phys. Fluids 34 (3) (2022) 033315.
[30] C. Stow, M. Hadfield, An experimental investigation of fluid flow resulting from the impact of a water drop with an unyielding dry surface, Proceedings of the Royal Society of London. A. Mathematical and Physical Sciences 373 (1755) (1981) 419–441.
[31] C. Mundo, M. Sommerfeld, C. Tropea, Droplet-wall collisions: experimental studies of the deformation and breakup process, Int. J. Multiph. Flow 21 (2) (1995) 151–173.
[32] J.C. Bird, S.S. Tsai, H.A. Stone, Inclined to splash: triggering and inhibiting a splash with tangential velocity, New J. Phys. 11 (6) (2009) 063017.
[33] J. Hao, J. Lu, L. Lee, Z. Wu, G. Hu, J. Floryan, Droplet splashing on an inclined surface, Phys. Rev. Lett. 122 (5) (2019) 054501.
[34] L. Xu, W.W. Zhang, S.R. Nagel, Drop splashing on a dry smooth surface, Phys. Rev. Lett. 94 (18) (2005) 184505.
[35] C.J. Howland, A. Antkowiak, J.R. Castrejón-Pita, S.D. Howison, J.M. Oliver, R.W. Style, A.A. Castrejón-Pita, It's harder to splash on soft solids, Phys. Rev. Lett. 117 (18) (2016) 184502.
[36] D. Lohse, Fundamental fluid dynamics challenges in inkjet printing, Annu. Rev. Fluid Mech. 54 (2022) 349–382.
[37] M.-J. Thoraval, K. Takehara, T. Etoh, S.T. Thoroddsen, Drop impact entrapment of bubble rings, J. Fluid Mech. 724 (2013) 234–258.
[38] S. Popinet, Gerris: a tree-based adaptive solver for the incompressible Euler equations in complex geometries, J. Comput. Phys. 190 (2) (2003) 572–600.
[39] S. Popinet, An accurate adaptive solver for surface-tension-driven interfacial flows, J. Comput. Phys. 228 (16) (2009) 5838–5866.
[40] S. Popinet, A quadtree-adaptive multigrid solver for the Serre–Green–Naghdi equations, J. Comput. Phys. 302 (2015) 336–358.
[41] A.L. Yarin et al., Drop impact dynamics: splashing, spreading, receding, bouncing, Annu. Rev. Fluid Mech. 38 (1) (2006) 159–192.
[42] S.T. Thoroddsen, M.-J. Thoraval, K. Takehara, T. Etoh, Droplet splashing by a slingshot mechanism, Phys. Rev. Lett. 106 (3) (2011) 034501.
[43] C. Josserand, S.T. Thoroddsen, Drop impact on a solid surface, Annu. Rev. Fluid Mech. 48 (2016) 365–391.
[44] J. Philippi, P.-Y. Lagrée, A. Antkowiak, Drop impact on a solid surface: short-time self-similarity, J. Fluid Mech. 795 (2016) 96–135, https://doi.org/10.1017/jfm.2016.142.
[45] R. Cointe, J.L. Armand, Hydrodynamic impact analysis of a cylinder, J. Offshore Mech. Arct. 109 (3) (1987) 237–243.
[46] S.D. Howison, J.R. Ockendon, S.K. Wilson, Incompressible water-entry problems at small deadrise angles, J. Fluid Mech. 222 (1991) 215–230, https://doi.org/10.1017/S0022112091001076.
[47] W. Wang, C. Ji, F. Lin, X. Wei, J. Zou, Formation of water in oil in water particles by drop impact on an oil layer, Phys. Fluids 31 (3) (2019) 037107.
[48] S.D. Hoath, Fundamentals of inkjet printing: the science of inkjet and droplets, John Wiley & Sons, 2016.
[49] A.A. Castrejón-Pita, E.S. Betton, N. Campbell, N. Jackson, J. Morgan, T.R. Tuladhar, D.C. Vadillo, J.R. Castrejon-Pita, Formulation, quality, cleaning, and other advances in inkjet printing, Atomization and Sprays 31 (4).
[50] V. Sanjay, U. Sen, P. Kant, D. Lohse, Taylor-Culick retractions and the influence of the surroundings, J. Fluid Mech. 948 (2022) A14.
[51] V. Sanjay, S. Lakshman, P. Chantelot, J.H. Snoeijer, D. Lohse, Drop impact on viscous liquid films, J. Fluid Mech. 958 (2023) A25.
[52] Z. Yang, B. Ji, J.T. Ault, J. Feng, Enhanced singular jet formation in oil-coated bubble bursting, Nature Physics (2023) 1–7.
[53] M. Geri, B. Keshavarz, G.H. McKinley, J.W. Bush, Thermal delay of drop coalescence, J. Fluid Mech. 833 (2017) R3.